Peierls barriers of *a*-type edge and screw dislocations moving on basal and prismatic planes in magnesium

Andriy Ostapovets[1] and Olena Vatazhuk[2]

[1]*Central European Institute of Technology – Institute of Physics of Materials (CEITEC IPM)*
Academy of Sciences of the Czech Republic, Žižkova 22, Brno, Czech Republic

[2]*B. Verkin Institute for Low Temperature Physics and Engineering of the National Academy of Sciences of Ukraine*
47 Nauky Ave., Kharkiv, 61103, Ukraine
E-mail: vatazhuk@ilt.kharkov.ua

Exact shape of Peierls barriers are calculated for <*a*> edge and screw dislocation gliding on basal and prismatic planes in magnesium by using of several popular interatomic potentials. Comparison of these potentials is performed in order to describe their abilities and limitations. Stability of different types of dislocation cores are analyzed as well as their mutual transformations during dislocation slip. It was found that the Peierls stresses and barrier height are dependent on core type. It was concluded that transformations of dislocation cores along minimal energy paths have to be taken into account for development of analytical models of the slip in magnesium. The results are compared with available first-principles calculations.

1. Introduction

Magnesium (Mg) and its alloys are perspective lightweight materials [1] that are widely used in biomedical [2] and energy storage applications [3,4]. It crystallizes in hexagonal close packed (hcp) lattice and, similarly to other hcp materials, its plastic deformation is characterized by the presence of a variety of slip and twinning modes [5,6]. The main dislocations responsible for the plastic deformation by slip have Burgers vectors $1/3\langle11\bar{2}0\rangle$ and move predominantly by basal slip on the $\{0001\}$ planes containing the Burgers vector. However, basal slip alone is not able to accommodate the deformation along the *c*-direction of the hcp lattice. This implies that $\langle11\bar{2}0\rangle\{10\bar{1}0\}$ prismatic and $\langle11\bar{2}3\rangle\{11\bar{2}2\}$ pyramidal systems may be activated together with deformation twinning. It is important to emphasize that both prismatic and pyramidal slip systems are difficult to activate at room temperature. This leads to a significant activity of twinning and to a widespread belief that Mg is a hard-to-deform material, which limits its applicability as a construction material. The ways to improve the deformation characteristics of Mg include grain refinement [7,8] and alloying with rare-earth ele-

ments [9]. Both procedures are expensive and their application potential is thus limited. Understanding the slip processes controlling the thermally activated glide of dislocations in this material is thus an important task that can lead in the future to significant improvements of its ductility.

Atomistic calculations have been utilized in the past to calculate the critical resolved shear stresses (CRSS) to move the *a*-type dislocations on basal and prismatic planes, but these values are quite scattered. In particular, the reported ratios of CRSS (prismatic): CRSS (basal) vary from 100:1 to 8:1 [6,10,11]. Such variations are often attributed to a significant temperature dependence of the CRSS at low temperatures [12] as well as high temperatures [6]. The hardening processes are also important [10]. Direct molecular dynamics simulations of slip processes in Mg are still impractical due to limitations molecular dynamics timescale, despite lower activation energies to move the a-type dislocations in comparison to those typical for more open structures. In principle, this limitation may be circumvented by making the calculation at much higher stresses (and thus also strain rates) or higher temperatures than those typical for real deformation experiments, but it is not clear to what extent this change affects the results of

such calculations. A more elegant solution of this problem is to develop thermodynamic models of slip that provide the dependence of the activation enthalpy on the applied stress, its character and orientation. The most prominent models developed to date are those by Seeger [13], Dorn and Rajnak [14], Celli *et al*. [15], Koizumi *et al*. [16] and Suzuki *et al*. [17]. The adjustable parameters in these models have to be determined by higher-level calculations, typically by a number of molecular statics simulations of isolated dislocations under stress [18]. One such example is the model of thermally activated cross-slip in Mg alloys developed by Yasi *et al*. [19,20].

When the plastic deformation is controlled by dislocations overcoming large Peierls barriers, these models depend sensitively not only on the height of this barrier but on its entire shape [21]. The reason is that the activation enthalpy, which determines the velocity of the dislocation and thus the plastic strain rate, is obtained by integrating over the shape of the Peierls barrier. The calculations of the core structures of individual dislocations in Mg and the critical stresses to move these dislocations at 0 K (the Peierls stresses) can be found in Refs. 22–26. Nevertheless, the calculations of complete Peierls barriers and their dependencies on the applied stress are still rare [21,27].

The objective of this paper is to compare theoretical predictions of slip activity obtained from several popular interatomic potentials for Mg with the results of first principles calculations and experiments. The obtained results can be used for more deep understanding of low temperature plasticity of magnesium. As described above, they can be used for further development of thermodynamic models for magnesium plasticity in wide range of temperature. In Sec. 2, we review and compare lattice parameters, cohesive energies and elastic constants predicted by each potential. In Sec. 3, we investigate the stability and energies of generalized stacking faults on basal and prismatic planes and identify all metastable faults. The purpose of Sec. 4 is to identify all core structures of *a*-type edge and screw dislocations. In Sec. 5, we utilize the Nudged Elastic Band (NEB) [28–30] method to calculate the Peierls barriers for glide of the *a*-type edge and screw dislocations on basal

and prismatic planes. The most important findings are discussed in Sec. 6 which also concludes this paper.

2. Interatomic potentials and geometry of the simulation block

All calculations in this paper will be made using three popular empirical interatomic potentials for Mg of the Embedded Atom Method (EAM) type, developed by Liu *et al*. [31], Sun *et al*. [32] and Sheng *et al*. [33]. The molecular statics calculations as well as the energies and forces of individual images in the NEB calculations were obtained using the LAMMPS code [35] and visualized in OVITO [36]. Nudged elastic band calculations were performed by using of NEB atoms code [37]. Calculations were performed at 0 K. A comparison of lattice parameters, cohesive energies and elastic constants predicted by these potentials is given in Table 1. Here, we use an improved version of Mg–Mg interactions from a recent Mg–Y potential provided by Dr. Sheng (private communication) and, therefore, the values in Table 1 marked "Sheng *et al*. (private communication)" are slightly different from those reported in Ref. 33.

Let us consider a single isolated dislocation with the Burgers vector $\langle 11\bar{2}0 \rangle$ parallel to the *a*-axis of the crystal. If direction of the dislocation line is parallel to the *a*-axis, it is a screw dislocation that can move on both $\{0001\}$ basal and $\{1\bar{1}00\}$ prismatic planes, as well as on any other plane in the zone of the *a*-axis. However, if the dislocation line is parallel to $\langle 0001 \rangle$ (*c*-axis), it represents the *a*-type edge dislocation whose slip plane coincides with the prismatic $\{1\bar{1}00\}$ plane. The edge dislocation with basal glide plane has dislocation line along $[10\bar{1}0]$ direction.

For all calculations, the orientation of the atomic block is such that the direction of the dislocation line is always parallel to the *z*-axis. In the studies of the *a*-type edge dislocation moving on the basal plane, the *x*-axis is parallel to the $[\bar{1}2\bar{1}0]$ direction and the *y*-axis parallel to the $[10\bar{1}0]$ direction. The *x* axis was parallel to $[\bar{1}2\bar{1}0]$ and the *y*-axis parallel to the $[0001]$ direction in the case of prismatic slip of edge dislocation. The *x*-axis of block was parallel to $[10\bar{1}0]$ and *y*-axis parallel to $[0001]$ direction in the case of screw *a*-type dislocation.

Table 1. Fundamental predictions of the three EAM potentials that were used for all calculations in this paper

	Liu *et al*. [31]	Sun *et al*. [32]	Sheng *et al*. (private communication)	Experiment [34]
a [Å]	3.195	3.184	3.211	3.207
c/a	1.623	1.628	1.588	1.624
E_{coh} [eV]	−1.510	−1.528	−1.512	–
C_{11} [GPa]	65.56	69.43	60.54	63.5
C_{12} [GPa]	25.46	25.23	24.79	25.9
C_{13} [GPa]	21.76	16.00	20.35	21.7
C_{33} [GPa]	63.42	69.83	78.22	66.5
C_{44} [GPa]	17.93	12.76	20.16	18.4
C_{66} [GPa]	20.05	22.07	17.86	18.8

The simulation box used for calculations of dislocation structures had a cylindrical geometry, where the rotation axis of the cylinder was made to coincide with the z-axis and thus the direction of the dislocation line. The block size was equal to 3 periodical distances in the z-direction. In the perpendicular xy plane, the circular cross-section of the block was subdivided into the region I at $r/a \leq R$ and the region II at $R < r/a < R+3$, where R was chosen between 50 and 80 to minimize the impact of boundary conditions. The dislocation was inserted into the center of the box parallel to the z-axis by displacement all atoms in the regions I and II using the anisotropic elastic strain field of the dislocation obtained from Stroh's sextic formalism [38] (see also Ref. 39). The atoms corresponding to the region II were then fixed, while those in the region I were relaxed using a chosen interatomic potential. The periodic boundary conditions applied along the z-direction make the dislocation effectively infinite. At the same time, the thickness of the region II of the block in the radial direction is larger than the cut-off radius of atomic interactions and thus the relaxations of atoms in the region I are unaffected by the termination of the block in the xy plane.

3. Structure and stability of generalized stacking faults

We will first investigate the stability of generalized stacking faults by calculating the γ surfaces [40] using the three interatomic potentials for Mg. These were obtained by cutting a perfect crystal along the basal or prismatic planes and displacing the upper part relative to the lower by a number of discrete vectors **t** that span one unit cell in the plane of the cut. After each such displacement, all atoms were relaxed in the direction perpendicular to the plane of the cut. The energy of the fault was then determined as

$$\gamma(\mathbf{t}) = \frac{E(\mathbf{t}) - NE_{\mathrm{coh}}}{S}, \qquad (1)$$

where NE_{coh} is the potential energy of an unfaulted crystal comprising N atoms, $E(\mathbf{t})$ the potential energy of the block with the fault defined by the vector **t**, and S the area of the fault. The γ surfaces corresponding to planar faults on the basal and prismatic planes obtained using the potentials of Liu et al., Sun et al. and Sheng et al. are shown in Fig. 1.

The basal-plane γ surfaces are mapped by creating a series of planar faults using the fault vector $\mathbf{t}^B = 1/3[11\bar{2}0]t_1^B + [1\bar{1}00]t_2^B$, where $t_1^B, t_2^B \in [0,1]$. All three

potentials predict local minima and thus metastable stacking faults at $(t_1^B, t_2^B) = (1/2, 1/6)$, whose energies are given in Table 2. The prismatic-plane γ surfaces are generated by considering fault vectors $\mathbf{t}^P = 1/3[11\bar{2}0]t_1^P + [0001]t_2^P$ with $t_1^P, t_2^P \in [0,1]$. Here, only the potentials of Liu et al. and Sun et al. predict the existence of local minima, whereas the potential of Sheng et al. does not predict any metastable stacking fault. The positions of the minima predicted by the former potentials are not the same, in particular $(t_1^P, t_2^P) = (1/2, 1/10)$ for Liu et al. and $(t_1^P, t_2^P) = (1/2, 3/20)$ for Sun et al. The lack of metastable faults on the prismatic plane as predicted by the potential of Sheng et al. results in a hard prismatic slip for pure Mg when studied by this potential. However, this may not be a problem in studies of ordered Mg–Y alloys for which this potential was primarily constructed. The positions and energies of metastable stacking faults on the prismatic-plane γ surfaces are again summarized in Table 2.

The γ surfaces in Fig. 1 identify the positions of metastable stacking faults into which the dislocation can dissociate. All three potentials predict that the $1/3[11\bar{2}0]$ dislocation may dissociate on the basal plane into two partial dislocations with the Burgers vectors $1/3[10\bar{1}0]$ and $1/3[01\bar{1}0]$ with a stacking fault (SF) in between. A similar albeit more complicated dissociation of the $[11\bar{2}0]$ dislocation on the prismatic plane is predicted only by the potentials of Liu et al. and Sun et al. In particular, these are $1/3[11\bar{2}0] \rightarrow 1/30[5\,5\,\overline{10}\,3] + 1/30[5\,5\,\overline{10}\,\bar{3}] + \mathrm{SF}$ for the potential of Liu et al. and $1/3[11\bar{2}0] \rightarrow 1/60[10\,10\,\overline{20}\,9] + 1/60[10\,10\,\overline{20}\,\bar{9}] + \mathrm{SF}$ for the potential of Sun et al.

4. Dislocation core structures

In order to examine possible dislocation core structures, the origin of the elastic field of the dislocation (and thus the center of the dislocation) was inserted at different positions relative to the unit cell of the crystal in the xy plane and thus perpendicular to the line direction of the dislocation.

Three core structures of the a-type screw dislocations were found in our simulations. These are characterized as: (i) basal core (B) that is dissociated on the basal plane into two partials with a stacking fault ribbon in between, and (ii) two undissociated compact cores extended on the prismatic plane (C1 and C2). These are shown in Fig. 2 for all potentials considered in this paper. The potential of Liu et al. predicts the existence of only the C1 core in agreement with the results

Table 2. Positions and energies of metastable stacking faults on the γ surfaces of Mg obtained using the three potentials

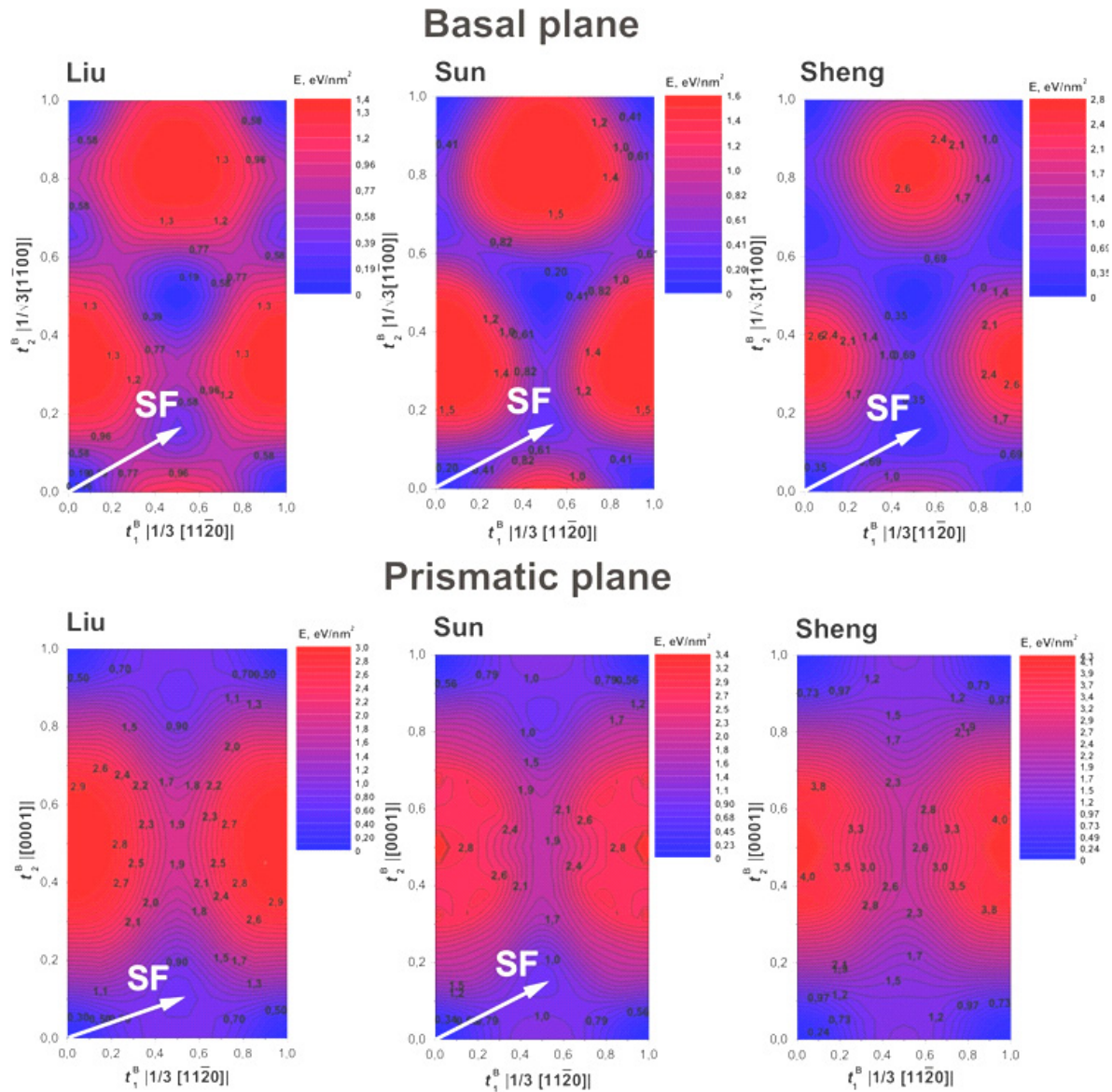|	Liu et al. [31]	Sun et al. [32]	Sheng et al. (private communication)
basal plane	$(t_1^B, t_2^B) = (1/2, 1/6)$ $\gamma = 0.3533$ eV/nm^2	$(t_1^B, t_2^B) = (1/2, 1/6)$ $\gamma = 0.2955$ eV/nm^2	$(t_1^B, t_2^B) = (1/2, 1/6)$ $\gamma = 0.1726$ eV/nm^2
prismatic plane	$(t_1^P, t_2^P) = (1/2, 1/10)$ $\gamma = 0.733$ eV/nm^2	$(t_1^P, t_2^P) = (1/2, 3/20)$ $\gamma = 0.835$ eV/nm^2	no metastable fault

Fig. 1. (Color online) γ surfaces representing the energies of generalized stacking faults on the (0001) basal plane (upper panels) and on the $(10\bar{1}0)$ plane (lower panels) obtained using the potentials of Liu *et al.*, Sun et al. and Sheng *et al*. The vectors marked SF represent the fault displacements **t** that create metastable stacking faults.

reported previously by Yasi *et al.* [20], whereas all three cores were found using the potential of Sun *et al.* The relative energies of these three cores are $E(C2) > E(C1) > E(B)$ which show that the dislocation dissociated on the basal plane is the most stable. The only core predicted by the potential of Sheng *et al.* of the *B*-type.

The core structures of *a*-type edge dislocations are shown in Fig. 3. The calculations made using all three potentials show that the dislocation is dissociated into two partials on the basal plane. The width of the intermediate stacking fault ribbon is the smallest for the potential of Liu *et al.* the largest for the potential of Sheng *et al.* As expected, this sequence agrees inversely with the ordering of basal-plane stacking fault energies obtained from the γ surfaces in Sec. 3.

5. Peierls barriers and stresses

We have utilized the NEB method to determine the minimum energy path of a dislocation between two equivalent positions in the lattice. For this purpose, we have first created two atomic blocks of the cylindrical geometry, as described earlier in this paper, which contain the dislocation at two different positions in the slip plane for which the total potential energy of the system is the same. These are the initial $(I = 0)$ and final $(I = M + 1)$ configurations (or "images") used in NEB simulations. The trial guess of the minimum energy path of the system represents a linear interpolation of the coordinates of atoms between the two fixed images using a set of M discrete intermediate (or movable) images. The minimum energy path was accepted if the fol-
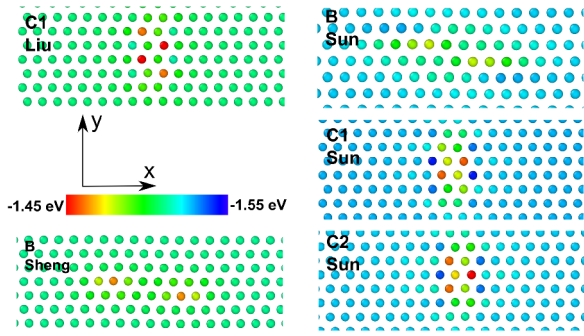
Fig. 2. (Color online) Dislocation cores of *a*-type screw dislocations. The *x* axis is parallel to $[10\bar{1}0]$ (*a*-direction) and the *y* axis parallel to $[0001]$ (*c*-direction). The atoms are color-coded according to the energy corresponding to each atom.

Fig. 3. (Color online) Dislocation cores of *a*-type edge dislocations. The *x*-axis is parallel to $[\bar{1}2\bar{1}0]$ and the *y*-axis is parallel to the $[10\bar{1}0]$ direction (figures on the left) or to $[0001]$ direction (figures on the right). The atoms are color-coded according to the energy corresponding to each atom.

lowing two conditions were satisfied simultaneously for the movable images [37]. The first criterion is $\max|\nabla_\perp E| < 0.01$ eV/Å, where $|\nabla_\perp E|$ is the L^2 norm of the force acting on each image in the direction perpendicular to the path. The second criterion is $\max|\Delta^2_{(I-1,I)} - \bar{\Delta}^2| < 10^{-6}$ nm², where $\Delta_{(I-1,I)}$ is the distance between images $I-1$ and I in the $3N$-dimensional space spanned by the coordinates of all atoms in the region I of the block and $\bar{\Delta}$ the average distance between two adjacent images. The last condition assures that the images are distributed equidistantly along the path but it does not necessarily guarantee that the positions of the dislocation along the path are uniform (for details, see [37]).

The shape of the Peierls barrier can be related to the magnitude of the Peierls stress by a well-known formula

$$\sigma_P b = \max(dV/d\xi) \qquad (2)$$

where b is the magnitude of the Burgers vector of the dislocation, $V(\xi)$ the Peierls barrier and σ_P the Peierls stress. Here ξ is the position of the dislocation that is zero in the initial configuration and reaches its maximum in the final configuration.

5.1. Basal slip

The Peierls barriers for basal slip of the *a*-type screw dislocations are shown in Figs. 4(a),(b) for the *B*- and *C*1-type dislocation cores, respectively. For all potentials considered, the Peierls barriers for the *B*-type core are about 3 orders of magnitude lower than those for the *C*1 core, which is not surprising owing to the large spreading of the former in the slip plane. The motion of the *B*-type core dislocation takes place without changes of core type.

The Peierls stresses for the *B*-type core dislocations are 3.9 MPa and 2.4 MPa for the Sun and Sheng potentials, respectively. The first value is comparable with the value of 3.6 MPa reported for the Sun potential by Yasi *et al.* [26] and obtained by a direct measurement of the stress necessary
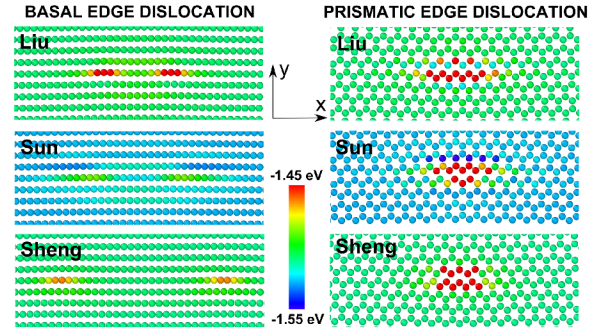
for dislocation motion. These values are somewhat lower than 9.6–13.1 MPa obtained from the orbital-free density functional method [27]. The Peierls barriers for the *C*1-type cores, shown in Fig. 4(b), exhibit a local minimum in the middle of the path for the potential of Sun *et al.* and a very shallow minimum for the potential of Liu *et al.* These minima correspond to the *B*-type core that is metastable for the Sun potential. However, no such core was found in Sec. 3 using the Liu potential, which is presumably due to a very shallow stability well of its Peierls potential (see Fig. 4(b)). The Peierls stresses obtained from the lower panels of Fig. 4(b) using Eq. (2) are 1494 MPa and 539 MPa for the Liu and Sun potentials, respectively. These values are more than two orders of magnitude higher than the stresses for the *B*-type core. However, they can affect the plastic deformation of Mg. The core transformation between the *B*-type to *C*1-type would happen during cross-slip of dislocation between prismatic and basal slip systems. These high values of stress are necessary only in order to initiate cross-slip. Subsequent dislocation glide needs much lower stresses and certainly is not accompanied by mutual core transformations.

The Peierls barriers for basal slip of the a-type edge dislocations are shown in Fig. 5. These are very low for the Sun and Sheng potentials as compared to the barrier obtained from the potential of Liu *et al.* There are no intermediate minima along the Peierls barrier for any potential which is consistent with the finding that the edge dislocation adopts a dissociated *B*-type core where the two partial dislocations correspond to the positions of the metastable stacking faults of the γ surfaces calculated in Sec. 3. The Peierls stresses obtained from the shapes of the Peierls barriers in Fig. 5 are 15.38 MPa for Liu, 0.21 MPa for Sun and 0.06 MPa for Sheng potentials. These values are in agreement with those previously reported in Ref. 27 which give the values of 14 MPa and 0.3 MPa for the Liu and Sun potentials, respectively.
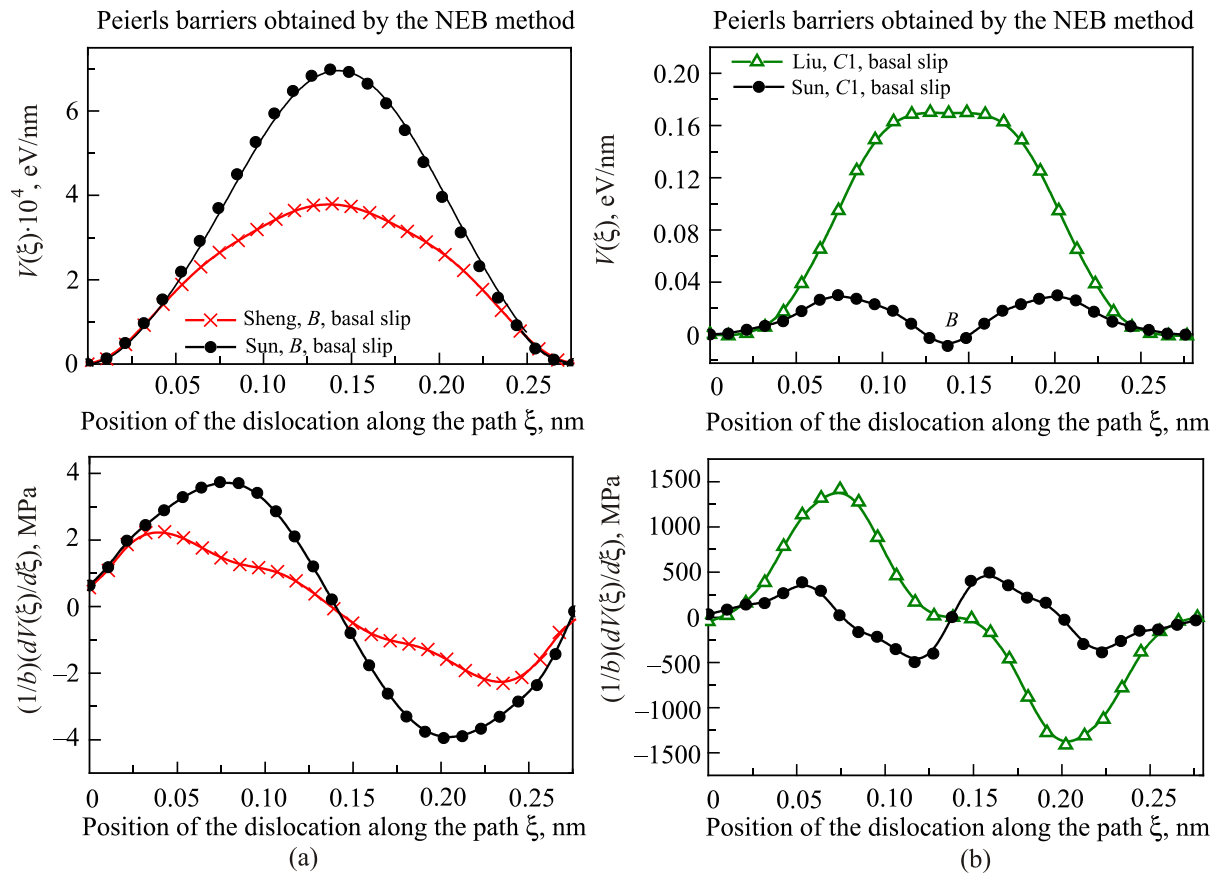
Fig. 4. (Color online) Peierls barriers for the *a*-type screw dislocation with *B*-type core (a), and *C*1-type core, moving on the basal plane (b). Additional minima in the central part of path can correspond to metastable core configurations. These configurations are marked by corresponding letters.

5.2. Prismatic slip

In Fig. 6(a), we plot the Peierls barriers for *a*-type screw dislocations originally adopting the *B*-core type moving on the prismatic plane as calculated using the potentials of Sun *et al.* and Sheng *et al.* There is no intermediate minimum on the Peierls barrier for the Sheng potential, which is consistent with the lack of metastable stacking faults on the γ surfaces calculated for this potential in Sec. 3. On the contrary, the Peierls barrier obtained by the potential of Sun *et al.* shows a deep intermediate minimum in the middle of the path which corresponds to the *C*2-type core. The Peierls stresses derived from the curves are the following. The stresses are 784 MPa and 3866 MPa for the Sun and Sheng potentials, respectively. The Peierls barriers for the *a*-type screw dislocation moving on the prismatic plane and having originally the *C*1-type core
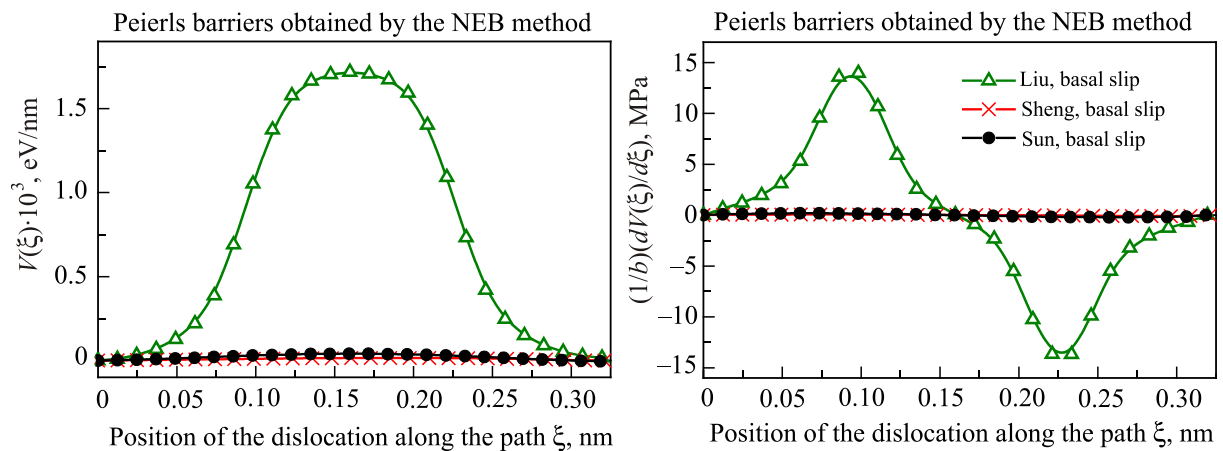

Fig. 5. (Color online) Peierls barriers for the *a*-type edge dislocation with the *B*-type core moving on the basal plane.
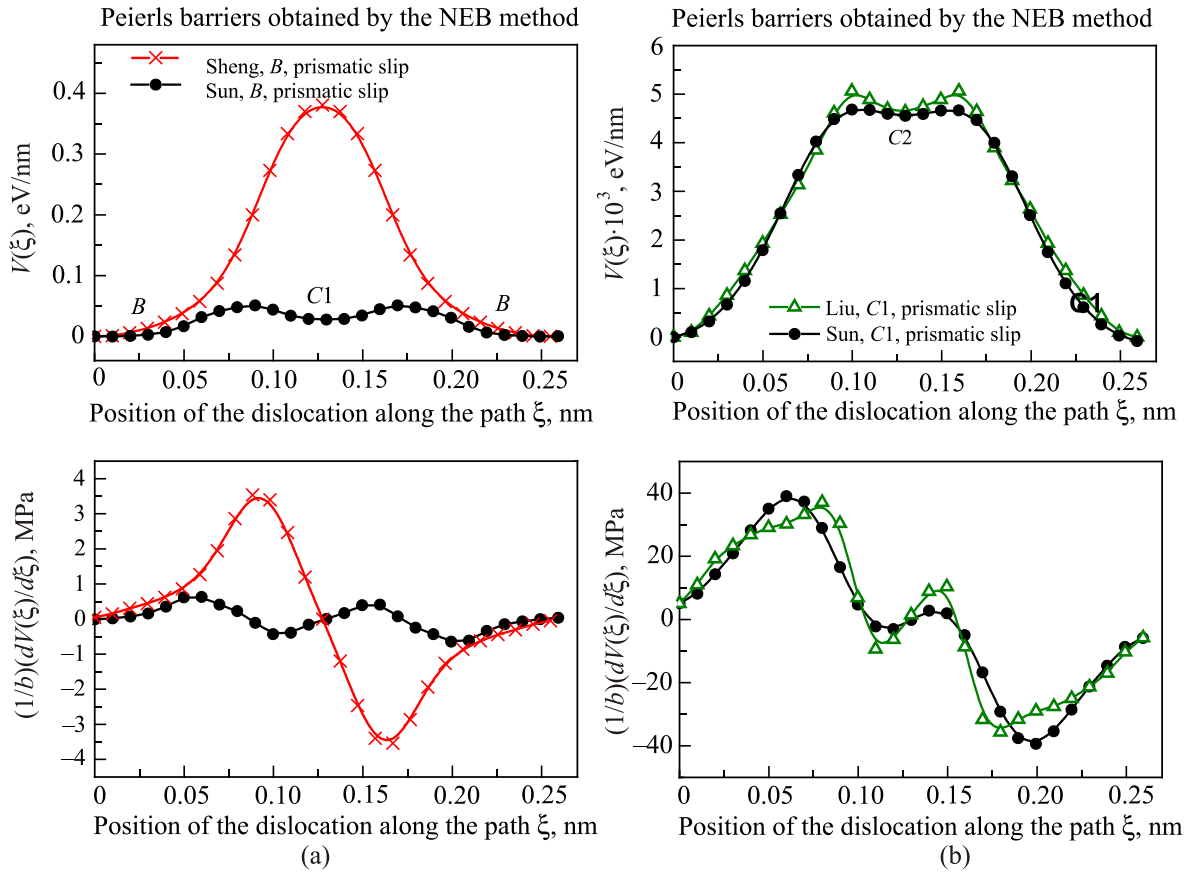
Fig. 6. (Color online) Peierls barriers for the *a*-type screw dislocation with *B*-type core (a), and *C*1-type core (b), moving on the prismatic plane. Additional minima in the central part of path can correspond to metastable core configurations. These configurations are marked by corresponding letters.

are shown in Fig. 6(b). For both potentials Liu *et al.* and Sun *et al.*, there are intermediate minima along the path which correspond to the transformation of the core to the metastable *C*2-type core. The Peierls stresses estimated from these potentials using Eq. (2) are 40 MPa and 42 MPa for Liu and Sun potentials, respectively.

The Peierls barriers for the *a*-type edge dislocation moving on the prismatic plane are shown in Fig. 7. Similar to the screw dislocations, the height of the barrier is much larger for the Sheng potential than for the Liu and Sun potentials. This is consistent with the small core of a prismatic edge dislocation shown for the Sheng potential in Fig. 3 as compared to the other two potentials. It also correlates well with large energies of stacking faults represented by the γ surface for this potential in Sec. 3. The corresponding Peierls stresses are 19.0 MPa, 19.1 MPa and 265.6 MPa for Liu, Sun and Sheng potentials, respectively.

In Table 3, we show the Peierls stresses calculated using the three EAM potentials and their comparison with the results of DFT calculations [27]. For the *a*-type screw dislocation, the DFT calculations predict easy glide on the basal plane, whereas prismatic slip requires roughly a factor of 4 larger Peierls stress. This trend is captured by the potentials of Sun *et al.* and Sheng *et al.*, where the

Peierls stresses obtained from the Sun potential are very close to the DFT values. The potential of Liu *et al.* predicts easier glide of the screw dislocation on the prismatic plane, which disagrees with DFT calculations. In the case of the *a*-type edge dislocation, the DFT calculations show a strong preference for basal slip, which is in agreement with the predictions made from the potentials of Sun *et al.* and Sheng *et al.* Again, the Peierls stresses obtained from the potential of Sun *et al.* are the closest to the DFT values. The potential of Liu *et al.* gives a marginal prefe-

Table 3. The Peierls stresses calculated by the three EAM potentials and their comparison with DFT calculations [27]. The numbers in bold are the lower of the two values for each dislocation and determine the primary slip plane that agrees with DFT calculations. All values are in MPa

		Liu *et al.*	Sun *et al.*	Sheng *et al.*	DFT
a-screw	basal slip	1493	**4.0**	**2.43**	**10.6**
	prismatic slip	**39.7**	41.5	3866	42.0
a-edge	basal slip	15.4	**0.2**	**0.06**	**0.6**
	prismatic slip	19.0	19.1	265.6	12.6

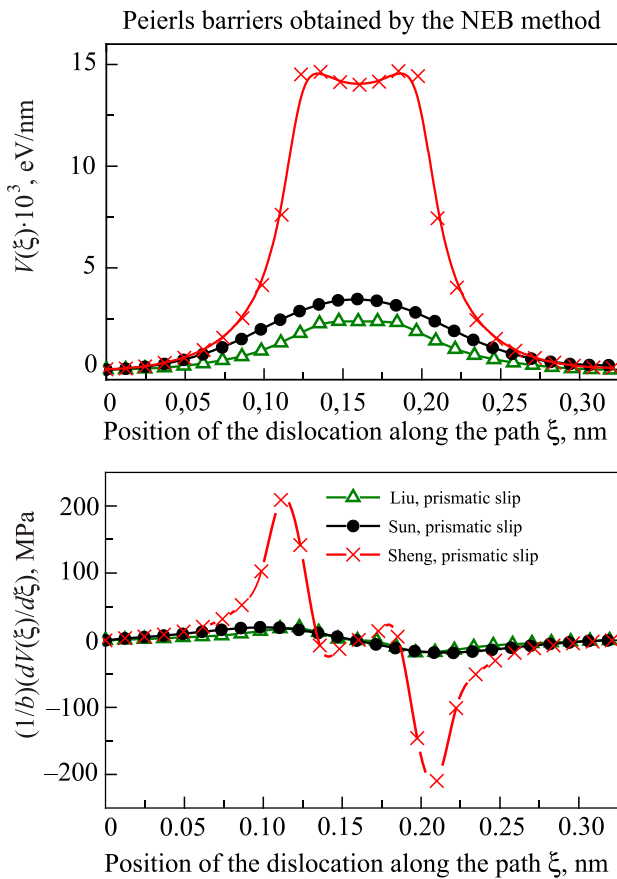## Peierls barriers obtained by the NEB method

Fig. 7. (Color online) Peierls barriers for the *a*-type edge dislocation moving on the prismatic plane.

rence for the basal slip which again does not agree with overwhelming preference towards the basal slip predicted by DFT calculations.

6. Conclusions

We compare Peierls barriers shapes predicted by three popular EAM potentials for magnesium. All three considered potentials show different behavior. The basal slip is hard for Liu potential. In contrast Sheng potential result in very hard prismatic slip. Both basal and prismatic slip system can be activated with Sun potential.

Among three potentials, the Sun *et al.* potential provides the best agreement with experimental data and data obtained from *ab-initio* calculations.

Variety of stable and metastable dislocation core are predicted by considered potentials. Dislocation cores transform to each other during dislocation slip. These transformations are often connected to dislocation cross-slip between basal and prismatic glide planes. The Peierls stresses and barrier height are dependent on core type. Peierls barriers obtained by NEB often have additional minima in their upper part. These minima correspond to metastable core types and the energy barrier between these core can be interpreted as barrier for cross-slip. The whole shapes of

energy barriers for cross-slip are reported first time. Transformations of dislocation cores along minimal energy paths have to be taken into account for development of analytical models of the slip in magnesium.

1. M.M. Avedesian and H. Baker, *Magnesium and Magnesium Alloys*, ASM International, Materials Park, OH (1999).
2. F. Witte, *Acta Biomater.* **6**, 1680 (2010).
3. A.M. Jorge, Jr., E. Prokofiev, G. Ferreira de Lima, E. Rauch, M. Veron, W.J. Botta, M. Kawasaki, and T.G. Langdon, *Int. J. Hydrogen Energy* **38**, 8306 (2013).
4. J. Cermak and L. Kral, *J. Power Sourc.* **214**, 208 (2012).
5. J.W. Christian and S. Mahajan, *Prog. Mater. Sci.* **39**, 1 (1995).
6. A. Chapius and J.H. Driver, *Acta Mater.* **59**, 1986 (2011).
7. S. Biswas, S.S. Dhinwal, and S. Suwas, *Acta Mater.* **58**, 3247 (2010).
8. P. Molnar and A. Jager, *Philos. Mag.* **93**, 3612 (2013).
9. S. Sandlobes, M. Friak, J. Neugebauer, and D. Raabe, *Mater. Sci. Eng. A* **576**, 61 (2012).
10. W.B. Hutchinson and M.R. Barnett, *Scripta Mater.* **63**, 737 (2010).
11. H. Wang, B. Raeisinia, P.D. Wu, S.R. Agnew, and C.N. Tome, *Int. J. Solid. Struct.* **47**, 2905 (2010).
12. F.F. Lavrent'ev, Yu.A. Pokhil, and V.I. Startsev, *Strength Mater.* **4**, 1216 (1972).
13. A. Seeger, *Philos. Mag.* **1**, 651 (1956).
14. J.E. Dorn and S. Rajnak, *Trans. AIME* **230**, 1052 (1964).
15. V. Celli, M. Kabler, T. Ninomiya, and R. Thomson, *Phys. Rev.* **131**, 58 (1963).
16. H. Koizumi, H.O.K. Kirchner, and T. Suzuki, *Acta Metall. Mater.* **41**, 3483 (1993).
17. T. Suzuki, H. Koizumi, and H.O.K. Kirchner, *Acta Metall. Mater.* **43**, 2177 (1995).
18. R. Gröger and V. Vitek, *Acta Mater.* **56**, 5426 (2008).
19. J.A. Yasi, L.G. Hector, Jr., and D.R. Trinkle, *Acta Mater.* **59**, 5652 (2011).
20. J.A. Yasi, L.G. Hector, Jr., and D.R. Trinkle, *Acta Mater.* **60**, 2350 (2012).
21. R. Gröger and V. Vitek, *Acta Mater.* **61**, 6362 (2013).
22. D.J. Bacon and D.J. Martin, *Philos. Mag.* **43**, 883 (1981).
23. M.H. Liang and D.J. Bacon, *Philos. Mag.* **53**, 181 (1986).
24. M.H. Liang and D.J. Bacon, *Philos. Mag.* **53**, 205 (1986).
25. M. Ghazisaedi and D.R. Trinkle, *Acta Mater.* **60**, 1287 (2012).
26. J.A. Yasi, T. Nogaret, D.R. Trinkle, Y. Qi, L.G. Hector, Jr., and W.A. Curtin, *Modelling Simul. Mater. Sci. Eng.* **17**, 055012 (2009).

27. I. Shin and E.A. Carter, *Int. J. Plasticity* **60**, 58 (2014).

28. H. Jonsson, G. Mills, and K.W. Jacobsen, in: *Classical and Quantum Dynamics in Condensed Phase Simulations*, B.J. Berne (ed.), World Scientific, Singapore (1998), p. 385.

29. G. Henkelman, and H. Jonsson, *J. Chem. Phys.* **113**, 9901 (2000).

30. G. Henkelman, B.P. Ubernaga, and H. Jonsson, *J. Chem. Phys.* **113**, 9978 (2000).

31. X.Y. Liu, J.B. Adams, F. Ercolessi, and J.A. Moriarty, *Model. Simul. Mater. Sci. Eng.* **4**, 293 (1996).

32. D.Y. Sun, M.I. Mendelev, C.A. Becker, K. Kudin, T. Haxhimali, and M. Asta, *Phys. Rev. B* **73**, 024116 (2006).

33. Z. Pei, L.-F. Zhu, M. Friak, S. Sandlobes, J. von Pezold, H.W. Sheng, C.P. Race, S. Zaefferer, B. Svendsen, D. Raabe, and J. Neugebauer, *New J. Phys.* **15**, 043020 (2013).

34. I.N. Francevich, F.F. Voronov, and S.A. Bakuta, *Uprugie Postojannye i Moduli Uprugosti Metallov i Nemetallov*, Naukova dumka, Kiev (1982).

35. S. Plimpton, *J. Comp. Phys.* **117**, 1 (1995).

36. A. Stukowski, *Model. Simul. Mater. Sci. Eng.* **18**, 015012 (2010).

37. R. Gröger and V. Vitek, *Model. Simul. Mater. Sci. Eng.* **20**, 035019 (2012).

38. A.N. Stroh, *J. Math. Phys.* **41**, 77 (1962).

39. J.P. Hirth and J. Lothe, *Theory of Dislocations*, New York, McGraw-Hill (1968).

40. V. Vitek, *Philos. Mag. A* **18**, 773 (1968).